JOURNAL OF GEOPHYSICAL RESEARCH: SPACE PHYSICS, VOL. 118, 3568–3575, doi:10.1002/jgra.50284, 2013

Daytime altitude variations of the equatorial, topside magnetic field-aligned ion transport at solar minimum

A. G. Burrell,[1] R. A. Heelis,[2] and A. Ridley[1]

Received 18 February 2013; revised 5 April 2013; accepted 17 April 2013; published 6 June 2013.

[1] Above the ion density peak, the interhemispheric transport of plasma plays an important role in shaping the spatial density distribution of the ionosphere. This study uses daytime observations of the ion drift, density, and composition near the geomagnetic equator from the Coupled Ion-Neutral Dynamics Investigation on board the Communication/Navigation Outage Forecasting System satellite, for the period of extremely low solar activity present in 2008 and 2009, to explore the altitude variation in interhemispheric transport at heights reaching up to the O^+/H^+ transition height. These observations revealed that the physical processes leading to interhemispheric transport do not change with altitude. These processes include forcing from the lower thermosphere, $\mathbf{E} \times \mathbf{B}$ drift, and chemical processes. Their longitudinal variations combine with the structure of the geomagnetic field to cause the differences in interhemispheric transport seen in different longitude regions. At all longitudes, the quantity of plasma crossing the geomagnetic equator depends strongly on ion density, which causes large changes to the altitude variations of the field-aligned plasma drift speed.

Citation: Burrell, A. G., R. A. Heelis, and A. Ridley (2013), Daytime altitude variations of the equatorial, topside magnetic field-aligned ion transport at solar minimum, *J. Geophys. Res. Space Physics*, *118*, 3568–3575, doi:10.1002/jgra.50284.

1. Introduction

[2] The regionof the ionosphere that lies between the ion density peak and the O^+/H^+ transition height is commonly known as the topside ionosphere. The plasma in this region is highly magnetized, allowing it to move readily along the magnetic field lines. The field-aligned drift of plasma across the geomagnetic equator, known as interhemispheric transport, has been the subject of previous investigations using both direct observations [*Venkatraman and Heelis*, 2000; *Chao et al*., 2004; *Burrell et al*., 2011, 2012] and inferences based on measurements of ion composition [*West and Heelis*, 1996; *West et al.*, 1997], ion temperature [*Su et al.*, 1998; *Venkatraman and Heelis*, 1999], and electron density [*Tulasi Ram et al.*, 2009; *Chen et al.*, 2009].

[3] The goal of this paper is to describe the altitude variations of the field-aligned drift in the topside ionosphere at different seasons and longitudes for low solar activity conditions. Past studies of topside field-aligned plasma drifts have focused on the drifts at a particular altitude, due to either the desire to explore other variations or the lack of measurements at a wide range of altitudes. Altitude variations could then only be inferred through latitude variations or through observations of other ion characteristics. This study explores the relative roles of the physical drivers causing interhemispheric transport using direct measurements of ion density and drift at all longitudes during the day at the geomagnetic equator. The characteristics of the interhemispheric transport presented in this paper will aid ionospheric characterization and prediction efforts.

2. Data

[4] Observations for this investigation were obtained from the Coupled Ion-Neutral Dynamics Investigation (CINDI) mission on board the Communication/Navigation Outage Forecasting System (C/NOFS) satellite [*de la Beaujardière et al*., 2004] during the solar minimum between the 23rd and 24th solar cycles. The C/NOFS satellite was launched on 16 April 2008 into a low Earth orbit with an inclination of 13° and an orbital period of about 97 min. During this period, the satellite orbit had a perigee of 400 km and an apogee near 860 km. This orbit allowed the orbital plane to precess 24 h in local time over a period of 3 months. Two instruments from the CINDI mission were used in this study: the retarding potential analyzer and the ion drift meter [*Heelis and Hanson*, 1998]. These instruments provided the three-dimensional ion velocity, converted into magnetic coordinates using the International Geomagnetic Reference Field (IGRF) [*Maus et al*., 2005], as well as the ion density, temperature, and composition. The field-aligned ion flux was computed by multiplying the measured field-aligned ion drift by the measured ion density.

[1]Department of Atmospheric, Oceanic and Space Sciences, University of Michigan, Ann Arbor, Michigan, USA.
[2]William B. Hanson Center for Space Sciences, The University of Texas at Dallas, Richardson, Texas, USA.

Corresponding author: A. G. Burrell, Department of Atmospheric, Oceanic and Space Sciences, University of Michigan, 2128 Space Research Bldg., Ann Arbor, MI 48109-2143, USA. (agburr@umich.edu)

2169-9380/13/10.1002/jgra.50284

Table 1. Seasonal Date Ranges

Season	Starting Date	Ending Date
December solstice	14 Nov 2008	17 Feb 2009
Equinox	18 Feb 2009	21 Apr 2009
Equinox	21 Aug 2009	20 Oct 2009
June solstice	22 Apr 2009	20 Aug 2009

[5] The Formosa Satellite 3/Constellation Observing System for Meteorology, Ionosphere, and Climate (FORMOSAT-3/COSMIC or F3/C) satellites [*Cheng et al.*, 2006] were also used in this investigation. This constellation consists of six microsatellites that were launched on 15 April 2006. During the period of time covered in this study, the microsatellites had spread to achieve a longitudinal separation of 30°, with orbits at 800 km, inclinations of 72°, and an orbital period of 100 min. Measurements of the height of the ion density peak, h_mF_2, were taken from electron density profiles obtained from the GPS Occultation Experiment (GOX) instrument that flies on board every microsatellite.

2.1. Data Processing

[6] To ensure high data quality and optimal instrument performance, this study used observations taken between 14 November 2008 and 20 October 2009, when O^+ concentrations fell below 99%. Seasonal divisions, outlined in Table 1, were chosen to ensure complete spatiotemporal data coverage. The CINDI data were also restricted to times with Kp $\leq$ 3, corrected geomagnetic latitudes within 5° of the geomagnetic equator, and solar local times between 10:30 and 15:00. This local time selection allowed altitudes as high as 700 km to be included, as sufficient O^+ density was available to ensure the quality of the CINDI instrument performance. Longitude regions were chosen, as shown in the fourth panel of Figure 1, to group observations by similar magnetic declinations (which are denoted by orange contours) and similar offsets between the geographic and geomagnetic equators. The first to third panels of Figure 1 show the longitudinal variations of the O^+/H^+ transition height for the December solstice, equinox, and June solstice. The O^+/H^+ transition height typically falls at or above the maximum altitude, limiting this study to regions of O^+ dominance.

[7] After completing the data selection for the measured field-aligned ion drift, measured ion density, and calculated field-aligned flux, running medians of these ion characteristics were computed with respect to altitude. The running medians were computed every 1.6 km using a moving window width of 40 km. Error bars denoting the 25% and 75% quantiles were used to represent scatter in the data. Any median computed using less than 50 measurements was removed from the data set.

[8] Quality control of the F3/C h_mF_2 was performed to minimize the contribution of error introduced through the computation of the electron density profile from the GOX radio occultations. Unrealistic electron density profiles can occur when the horizontal electron density gradients are present or when the assumption of spherical symmetry made by the Abel inversion process is violated [*Yue et al.*, 2010]. The worst instances of physically unrealistic data were excluded by requiring a minimum altitude for h_mF_2 of 120 km.

[9] To examine the relationship between the apex ion characteristics and those at the magnetic flux tube feet, the F3/C h_mF_2 and N_mF_2 were paired with the CINDI ion medians computed for each longitude region and season. As illustrated in Figure 2, the h_mF_2 measurements in each hemisphere are ordered by magnetic inclination (magnetic latitude). This allows the dipole field lines to be traced from their apex altitude to the location of the h_mF_2. By tracing along field lines that peak at altitudes corresponding to the upper and lower limits of the CINDI running median window (marked by plus signs in Figure 2), corresponding magnetic latitude limits were found in the northern and southern hemispheres (marked in Figure 2 by $N_{max,min}$ and $S_{max,min}$, respectively). The northern and southern median h_mF_2 and N_mF_2 were then computed using all of the F3/C observations that fell between these limits. Finally, the conjugate h_mF_2 displacement was computed by subtracting the northern h_mF_2 median from the southern h_mF_2 median. Note that Figure 2 shows the pairing between F3/C h_mF_2 and CINDI ion medians for a single apex altitude of 420 km. This pairing process is performed at all apex altitudes from 400 to 700 km.

2.2. Analysis

[10] If it is assumed that the ionosphere is in a quasi steady state and the ion and electron populations are ideal gases, the field-aligned drifts ($v_{\|}$) can be expressed analytically using equation (1) [*Heelis*, 2004]:

$$v_{\|} = u_{\|} - \frac{g_{\|}}{\nu_{\text{in}}} - \frac{k_B}{nm_i\nu_{\text{in}}}\nabla_{\|}n(T_i + T_e). \quad (1)$$

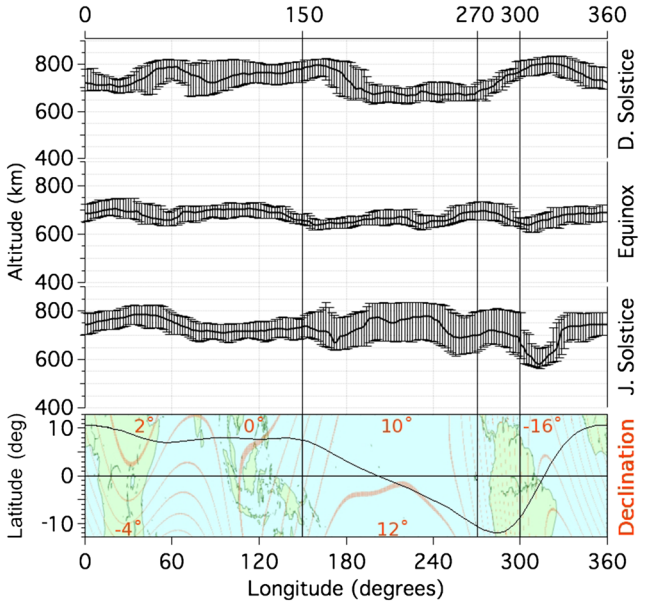

Figure 1. Longitudinal variations of the O^+/H^+ transition height for the (first panel) December solstice, (second panel) equinox, and (third panel) June solstice seasons as well as (fourth panel) a map of the geographic region covered by the C/NOFS satellite with magnetic declination (orange contours and labels) provided by IGRF. Four longitude regions are separated by vertical lines, and their longitude limits are shown on the top axis.

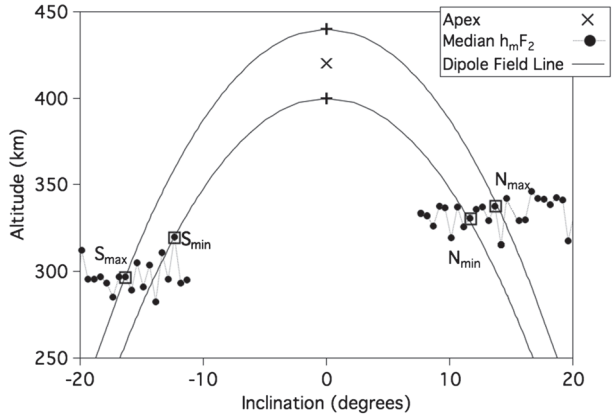

Figure 2. Pairing apex altitudes with northern and southern F3/C h_mF_2.

[11] In this equation, $u_{\|}$ is the field-aligned component of the neutral wind, $g_{\|}$ is the field-aligned component of the gravitational acceleration, ν_{in} is the ion-neutral collision frequency, k_B is the Boltzmann constant, T_e and T_i are the electron and ion temperatures, m_i is the ion mass, and n is the total ion or electron number density. As equation (1) represents a scenario where competing forces are balanced, field-aligned plasma drifts will be seen when the field-aligned component of the plasma pressure gradient is not countered by the field-aligned contributions from collisions with neutral particles and gravity. At the geomagnetic equator, gravity has no field-aligned component. This leaves direct ion-neutral collisions and nonzero field-aligned plasma pressure gradients caused by hemispheric asymmetries in ion production and loss, ion and electron temperatures, and the neutral winds below the ion density peak to drive field-aligned plasma drifts. The presence of meridional $\mathbf{E} \times \mathbf{B}$ plasma drifts will also alter any existing field-aligned plasma pressure gradient.

[12] Thermospheric winds drive the field-aligned drifts through ion-neutral collisions both above and below the ion density peak. In the topside ionosphere, the ion-neutral collision frequency is low enough that direct collisional contributions to the field-aligned drift take place on timescales of several hours, and thus, the ion drifts are much more responsive to field-aligned pressure gradients. At and below the ion density peak, however, the higher neutral density allows the neutral wind along the magnetic meridian to raise or lower the h_mF_2. When there are differences in conjugate ion number density associated with conjugate differences in the h_mF_2, these differences will result in field-aligned interhemispheric plasma transport [*Burrell and Heelis*, 2012].

[13] The h_mF_2 is also influenced by the meridional $\mathbf{E} \times \mathbf{B}$ drift, which moves plasma between flux tubes. At the geomagnetic equator, the meridional $\mathbf{E} \times \mathbf{B}$ drift is directed vertically. During the day, when this vertical/meridional $\mathbf{E} \times \mathbf{B}$ drift is directed upward, symmetric field-aligned drifts away from the flux tube apex (toward the geomagnetic poles) arise in response to the change in volume and gravitational acceleration that results from transporting the plasma vertically onto a larger magnetic flux tube. Known as the fountain effect, the transport of plasma away from the geomagnetic equator to higher latitudes alters the latitudinal variations of h_mF_2 and the peak ion density (N_mF_2). Although the meridional $\mathbf{E} \times \mathbf{B}$ drifts are not, on their own, capable of creating interhemispheric transport, the change in the flux tube volume as the plasma is transported upward or downward alters the field-aligned plasma pressure gradient. In the presence of existing interhemispheric transport, an increase or a decrease in the volume of the magnetic flux tube will respectively decrease or increase the existing field-aligned plasma pressure gradient.

[14] Ion production and loss processes alter the field-aligned plasma pressure gradient when there are hemispheric asymmetries in solar zenith angles or O/N_2 ratios. During the local time region used in this study, both photoionization and chemical loss processes are active. As altitude increases, however, the total ion density becomes increasingly influenced by the resonant charge exchange between the O^+ and H populations [*Hargreaves*, 1994]. Thus, it is expected that magnetic flux tubes that peak close to the O^+/H^+ transition height will show interhemispheric transport that is influenced by the changing composition [*Venkatraman and Heelis*, 2000].

[15] Longitude variations in the meridional $\mathbf{E} \times \mathbf{B}$ drift, lower thermospheric neutral winds, and O/N_2 ratio have been shown to be influenced by atmospheric tides. Several modes of nonmigrating tides and stationary planetary waves have been linked to a four-peaked longitudinal structure in thermospheric and ionospheric characteristics when these characteristics are viewed at a fixed local time [e.g., *Sagawa et al*., 2005; *Immel et al*., 2006; *Lin et al*., 2007; *Oberheide and Forbes*, 2008; *Forbes et al*., 2008]. Simulations have shown that this structure can be produced in the F_2 peak and daytime $\mathbf{E} \times \mathbf{B}$ drift by the combined influence of the diurnal eastward propagating nonmigrating tide with zonal wave number 3 (DE3) and the stationary planetary wave 4 (SPW4), the latter of which is generated by a nonlinear interaction between the DE3 and DW1 (diurnal westward propagating nonmigrating tide with zonal wave number 1) [*Pedatella et al.*, 2012]. These tides and planetary waves produce tidal structures in the lower thermosphere through upward wave propagation and in the ionosphere through electrodynamical coupling. Ion-neutral coupling also plays an important role in shaping the longitudinal structure in both the ionosphere and thermosphere, though coupling plays a secondary role during low solar activity conditions [*Wan et al.*, 2012]. Therefore, it is unsurprising that four-peaked longitudinal structures were seen in the field-aligned ion drifts by *Burrell et al.* [2012] near the bottom of the topside ionosphere. At higher apex altitudes, these structures may change, as the processes that introduce the four-peak variation vary with latitude and altitude.

[16] The field-aligned plasma pressure gradient term shown in equation (1) shows that hemispheric asymmetries in the plasma temperature as well as the plasma density may also contribute to the formation of interhemispheric transport. Rapid changes in the electron temperature have indeed been shown to cause field-aligned plasma drifts after sunrise [*Oyama et al.*, 1996], and adiabatic heating and cooling processes are important at night [*Venkatraman and Heelis*, 1999]. During the daytime, however, ion and electron populations closely approximate ideal gases [*Hargreaves*, 1994] and the field-aligned changes in the plasma density are

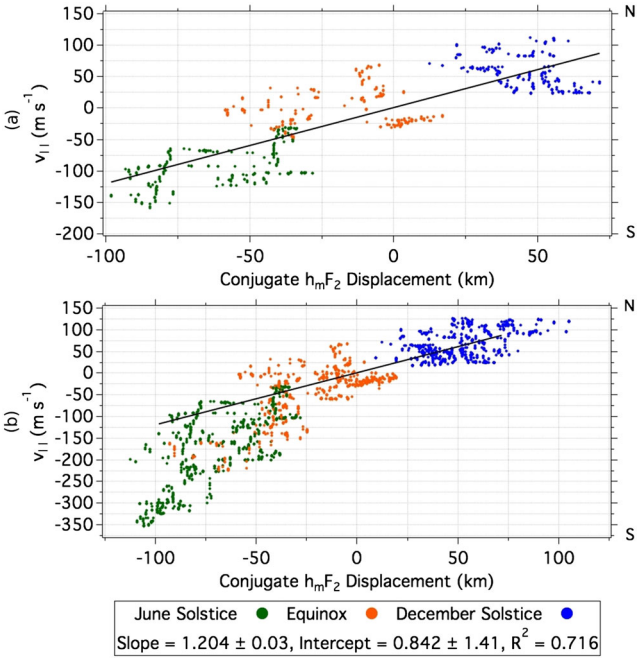

Figure 3. Correlation between the field-aligned ion drift and conjugate h_mF_2 displacement between 10:30 and 15:00 solar local times at the geomagnetic equator for altitudes (a) between 400 and 500 km and (b) between 400 and 700 km.

sufficient to infer the behavior of the field-aligned plasma pressure gradient.

3. Results and Discussion

[17] Past studies of interhemispheric transport have noted that below the O^+/H^+ transition height, field-aligned drifts are strongly correlated with processes in the lower thermosphere that affect the height and density of the F_2 peak [*Moffett and Hanson*, 1973; *Kutiev et al.*, 1980; *Heelis and Hanson*, 1980; *Burrell et al.*, 2012; *Burrell and Heelis*, 2012]. Above the O^+/H^+ transition height, however, the lighter H^+ ions are less amenable to transport across the magnetic equator [*Venkatraman and Heelis*, 2000]. As this study is limited to observations reaching up to the O^+/H^+ transition height (as shown previously in Figure 1), it is expected that lower thermospheric processes will dominate the contributions to the apex field-aligned drifts at all altitudes.

[18] Figure 3 investigates this hypothesis by exploring the relationship between the field-aligned drifts and the conjugate h_mF_2 displacement using median values computed in all four longitude regions outlined in Figure 1. Figure 3a includes measurements with apex altitudes below 500 km, as well as the best fit line computed from these measurements. Figure 3b includes measurements taken at apex altitudes below 700 km, as well as the best fit line from the lower altitudes plotted for comparison. In this and all other figures, the field-aligned drift is positive when directed toward the northern magnetic pole and negative when directed toward the southern magnetic pole. The conjugate h_mF_2 displacement is defined such that positive values indicate that the southern flux tube has a higher h_mF_2 than the northern flux tube, allowing the plasma to flow toward the northern magnetic pole in an effort to equalize the field-aligned plasma pressure gradient.

[19] Figure 3a shows that a strong linear correlation between the daytime field-aligned drift and the conjugate h_mF_2 displacement exists at all longitudes. This relationship is not as strong as it is at other local times, however, due to the presence of a strong meridional $\mathbf{E} \times \mathbf{B}$ drift directed vertically upward [*Stoneback et al.*, 2011] that peaks late in the morning. As previously discussed, the presence of this upward meridional $\mathbf{E} \times \mathbf{B}$ drift will decrease the magnitude of the field-aligned drifts.

[20] When the observations taken at higher altitudes are added, as shown in Figure 3b, large seasonal disparities can be seen. During the December solstice, data at all altitudes fall close to the lower altitude best fit line. During equinox and the June solstice, strong southbound field-aligned drifts suggest that the dependence of the ion drift on the conjugate h_mF_2 displacement changes at higher apex altitudes, possibly due to changes in the ion number density. Noting that the ion number density at the higher apex heights will be lower than that seen at lower apex heights and that the ion density reaches a maximum during equinox and a minimum during the June solstice, the relationship between the conjugate h_mF_2 displacement and the field-aligned ion flux is investigated in Figure 4.

[21] Figure 4 shows the field-aligned ion flux at the geomagnetic equator versus the conjugate h_mF_2 displacement using the same format as Figure 3. Figure 4a shows the low-altitude relationship, while Figure 4b shows all altitudes. Positive (negative) fluxes indicate northbound (southbound) transport. As was the case in Figure 3, Figure 4a shows a

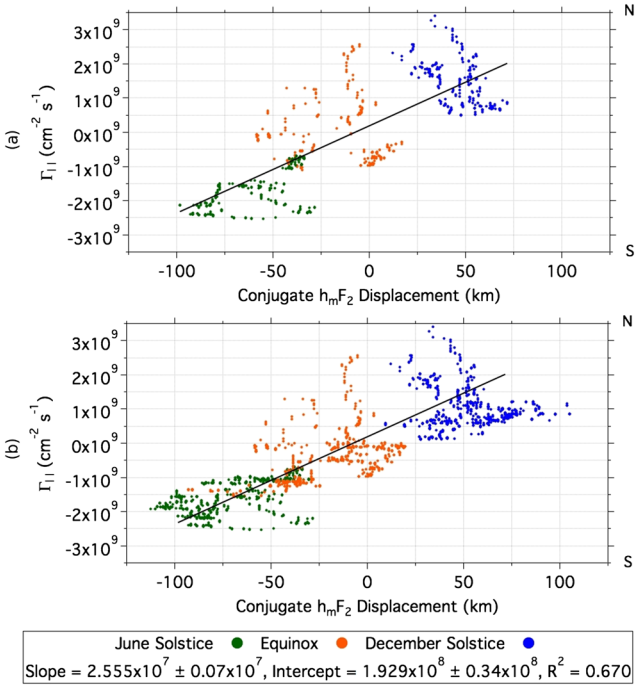

Figure 4. Correlation between the field-aligned ion flux and conjugate h_mF_2 displacement between 10:30 and 15:00 solar local times at the geomagnetic equator for altitudes (a) between 400 and 500 km and (b) between 400 and 700 km.

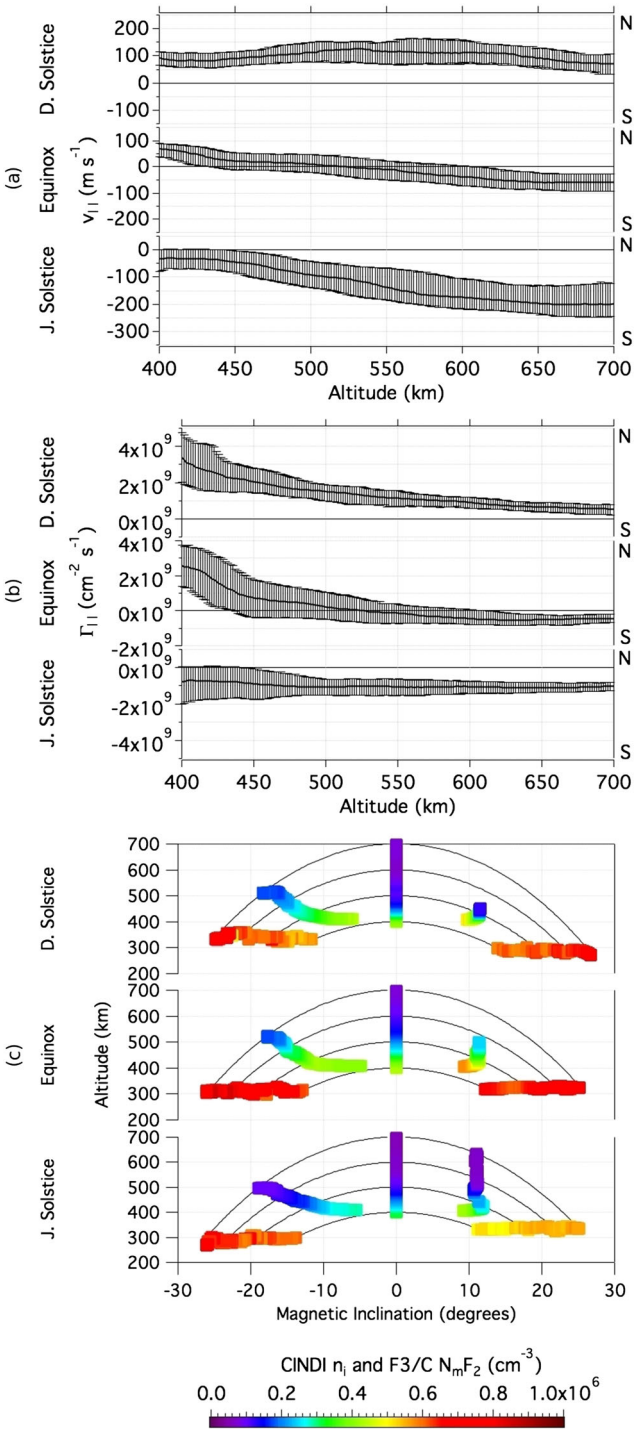

Figure 5. The altitude variations of the (a) field-aligned drift and (b) field-aligned flux within 5° of the geomagnetic equator as well as (c) the plasma density for 0°–150° longitude.

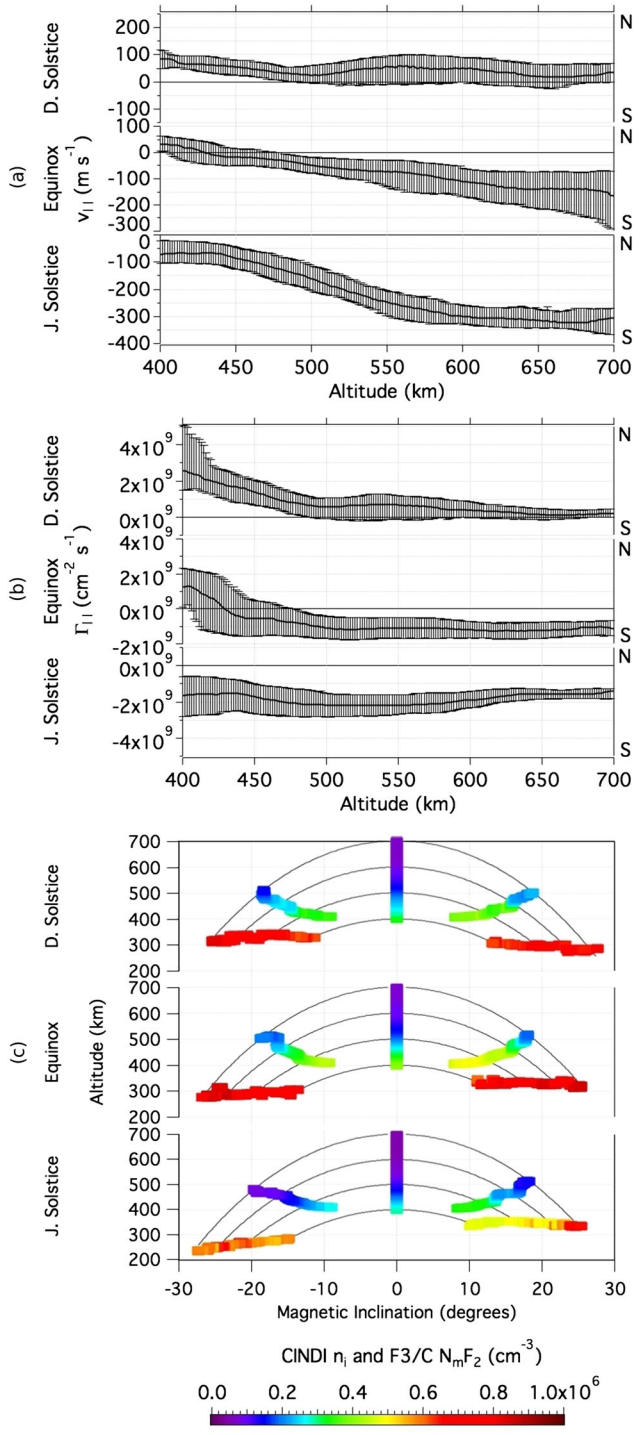

Figure 6. The altitude variations of the (a) field-aligned drift and (b) field-aligned flux within 5° of the geomagnetic equator as well as (c) the plasma density for 150°–270° longitude.

good correlation between the field-aligned plasma transport and the conjugate h_mF_2 displacement. However, comparing Figures 3b and 4b shows that while the lower altitude best fit line was clearly not appropriate at all altitudes for the field-aligned drift, it provides a much better representation of the relationship between the conjugate h_mF_2 displacement and the field-aligned flux. The goodness of fit between the lower altitude best fit line and the data at all altitudes was found to be 0.888, confirming the continued validity of the relationship between the field-aligned flux and the conjugate h_mF_2 at higher altitudes. This suggests that the topside interhemispheric ion flux is established just above the F peak by the hemispheric asymmetry in h_mF_2. Once established, the field-aligned ion drifts are determined by

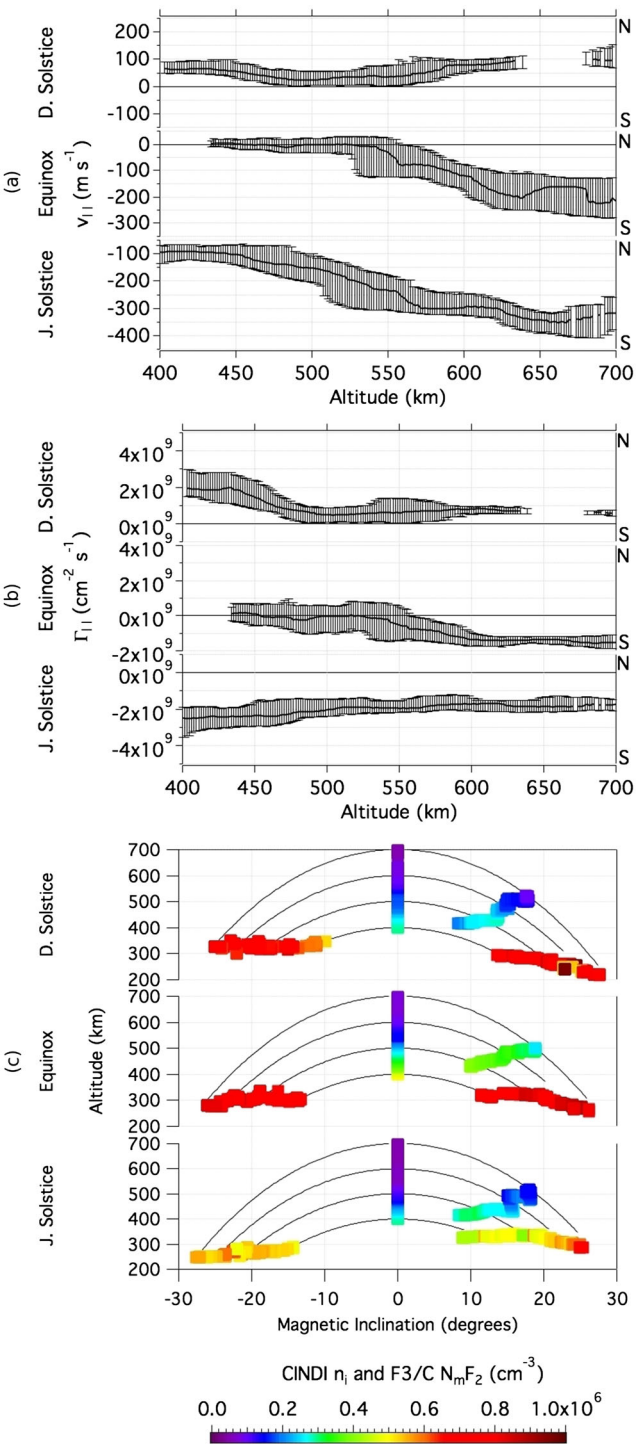

Figure 7. The altitude variations of the (a) field-aligned drift and (b) field-aligned flux within 5° of the geomagnetic equator as well as (c) the plasma density for 270°–300° longitude.

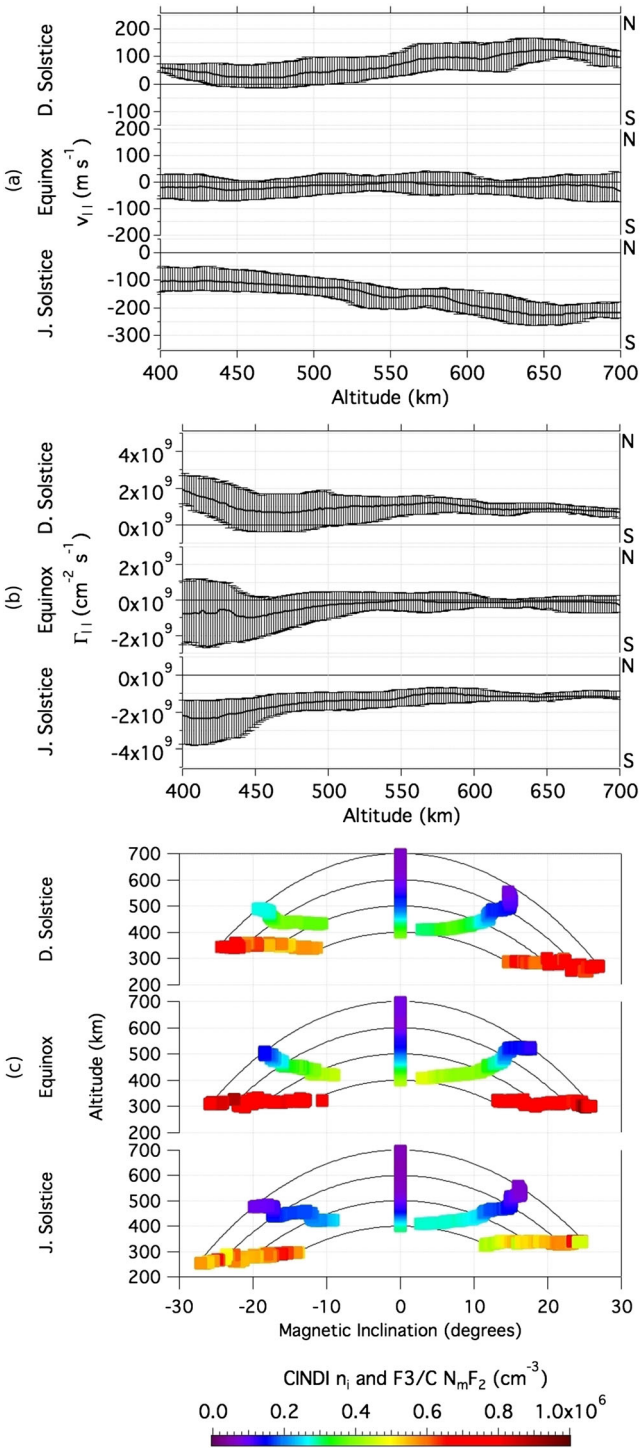

Figure 8. The altitude variations of the (a) field-aligned drift and (b) field-aligned flux within 5° of the geomagnetic equator as well as (c) the plasma density for 300°–360° longitude.

the distribution of ion density along the magnetic flux tube. Thus, the field-aligned drift increases at higher altitudes and is larger during seasons where the ion density is diminished, while the field-aligned flux maintains a similar relationship with the conjugate h_mF_2 displacement at all altitudes and seasons.

[22] Finally, the altitude variations of the interhemispheric transport in each of the four longitude regions shown in Figure 1 are presented in Figures 5–8. Figures 5a–8a show the field-aligned drift, Figures 5b–8b show the field-aligned flux, and Figures 5c–8c show the plasma density from both CINDI and F3/C. The plots in Figures 5c–8c show the F3/C

N_mF_2 at the h_mF_2, the CINDI ion density between $\pm 5°$ corrected magnetic latitudes at the field line apex, and the CINDI ion density between $\pm(5°–10°)$ corrected magnetic latitudes at their average altitude and inclination. Due to the satellite orbit, whose geographic range is shown in the fourth panel in Figure 1, complete coverage is not available in every longitude region. Figure 5 includes eastern longitudes where the declination is close to zero and the geomagnetic equator lies about 8° to the north of the geographic equator, Figure 6 encompasses the Pacific Ocean where the declination is positive and the geographic and geomagnetic equators intersect, Figure 7 covers the American continents and is characterized by rapid changes in declination as the geomagnetic equator dips to the south, and Figure 8 shows the western longitudes where the declination is negative and the geographic and geomagnetic equators intersect once again.

[23] The field-aligned drifts shown in Figures 5a–8a are well described by combining forcing from the altitude and latitude changes in ion density with the forcing from the neutral winds that raise or lower the h_mF_2, whose magnitude can be inferred by comparing the conjugate h_mF_2 shown in Figures 5c–8c. The largest field-aligned drifts are seen during the June solstice when the ion density is the lowest, the conjugate h_mF_2 displacement is large, and the latitude distribution of the ion density leads to larger ion densities in the hemisphere with the higher h_mF_2. A similar situation is seen at equinox, though the ion densities are highest during this season and conjugate h_mF_2 displacements are not omnipresent. At longitudes where both a conjugate h_mF_2 displacement and a hemispheric difference in the ion density distribution are present, the higher density occurs in the hemisphere with the higher h_mF_2. This is most easily seen between 150° and 270° longitudes (Figure 6), where the CINDI ion density measured off the geomagnetic equator is about 1.0×10^5 cm^{-3} greater in the northern hemisphere for the dipole field lines that peak at and below 600 km, and the F3/C h_mF_2 is typically above 300 km in the northern hemisphere and below 300 km in the southern hemisphere. Hemispheric differences in ion density are also clearly visible in Figure 5, and a large conjugate h_mF_2 displacement is present in Figure 7. Between 300° and 360° longitudes (Figure 8), very little hemispheric asymmetry is seen in the ion density or the h_mF_2. This is reflected in the field-aligned drift, which lies close to zero at all altitudes.

[24] Small field-aligned drifts are also seen at high altitudes during the December solstice between 0° and 270° longitudes (Figures 5 and 6). At these locations, the small drifts cannot be attributed to hemispheric symmetry. Considering only the altitudes where the CINDI measurements in both hemispheres were taken at comparable inclinations, the ion density above the h_mF_2 in the north is higher than it is in the south, in opposition to the conjugate h_mF_2 displacement. This indicates that a field-aligned plasma pressure gradient (formed by the conjugate h_mF_2 displacement, possibly in combination with other processes such as postsunrise photoionization) has succeeded in removing a large portion of the pressure gradient at the apex by transferring much of the plasma created in the southern hemisphere to the northern hemisphere.

[25] Looking at the field-aligned fluxes in Figures 5b–8b, it can be seen that the largest flux magnitudes and most rapid changes in flux are typically seen at altitudes below about 500 km. Exceptions occur at equinox between 270° and 300° longitudes (Figure 7) and at all longitudes during the June solstice. The lower flux magnitudes are expected during the June solstice, as the ion density (shown in Figures 5c–8c) is lowest during this season. At equinox, the ion density reaches a maximum, but the neutral winds that raise or lower the h_mF_2 are more hemispherically symmetric. Figure 7c shows that unlike those at other longitude regions, the conjugate h_mF_2 displacement increases dramatically for flux tubes that peak above 525 km. The abrupt change in conjugate h_mF_2 displacement is characteristic of this longitude region (which lies primarily to the south of the geographic equator and encompasses rapid changes in magnetic declination) and explains why the field-aligned flux magnitude increases with altitude in this longitude region but not elsewhere during equinox.

[26] At higher altitudes, the field-aligned flux changes much more slowly. Since the ionization production and loss rates fall dramatically with altitude, the greatest changes in ion density are caused by the field-aligned diffusive fluxes. If the ionosphere is in a quasi steady state, then the divergence of the ion flux will be zero. In the absence of a diverging ion flux, the plasma continuity equation requires that any decrease in ion density causes an increase in the ion drift. This is consistent with the observations of the field-aligned drifts in Figures 5a–8a, which show that the largest speeds are seen when the field-aligned flux in Figures 5b–8b changes the least with respect to altitude.

4. Conclusions

[27] This paper presents the climatology of altitude variations in the interhemispheric transport at the geomagnetic equator during the deep solar minimum that took place between the 23rd and 24th solar cycles. The physical processes that drive the field-aligned drifts close to the O^+/H^+ transition height were found to be the same as those that dominate closer to the h_mF_2, though the altitudinal changes in the total ion density played a more important role in determining the magnitude of the field-aligned drift at altitudes above about 500 km. At this point, the altitude variations in the field-aligned ion flux became small, leading the field-aligned drifts to increase in magnitude as the ion density decreased with increasing altitude. Thus, the largest field-aligned drifts were seen when the ion density was the lowest.

[28] The latitudinal distribution of the ion density also played a role in driving interhemispheric transport. When the ion density and h_mF_2 are both higher in one hemisphere, they work together to create an increased field-aligned plasma pressure gradient that drives plasma toward the opposite hemisphere. When the hemispheric ion density distribution and the conjugate h_mF_2 displacement were in opposition, however, the forcing from lower thermospheric neutral winds that raise and lower the h_mF_2 was the most influential physical process.

[29] **Acknowledgments.** This study was supported by AFOSR DDDAS grant FA9550-12-1-0401, as well as NASA grants NAS5-01068 and NNX10AT02G. The authors would like to thank Jeff Klenzing for his comments on this work and the F3/C orbital operation team at the National Space Organization (NSPO) and the University Corporation for Atmospheric Research (UCAR) for their roles in obtaining and distributing the F3/C data. NSPO is supported by the National Science Council of Taiwan.

[30] Robert Lysak thanks Koh-Ichiro Oyama and another reviewer for their assistance in evaluating this paper.

References

Burrell, A. G., and R. A. Heelis (2012), The influence of hemispheric asymmetries on field-aligned ion drifts at the geomagnetic equator, *Geophys. Res. Lett.*, *39*, L19101, doi:10.1029/2012GL053637.

Burrell, A. G., R. A. Heelis, and R. A. Stoneback (2011), Latitude and local time variations of topside magnetic field-aligned ion drifts at solar minimum, *J. Geophys. Res.*, *116*, A11312, doi:10.1029/2011JA016715.

Burrell, A. G., R. A. Heelis, and R. A. Stoneback (2012), Equatorial longitude and local time variations of topside magnetic field-aligned ion drifts at solar minimum, *J. Geophys. Res.*, *117*, A04304, doi:10.1029/2011JA017264.

Chao, C. K., S.-Y. Su, and H. C. Yeh (2004), Ion temperature crests and troughs in the morning sector of the low-latitude and midlatitude topside ionosphere, *J. Geophys. Res.*, *109*, A11303, doi:10.1029/2003JA010360.

Chen, G., J. Xu, W. Wang, J. Lei, and Y. Deng (2009), Field-aligned plasma diffusive fluxes in the topside ionosphere from radio occultation measurements by CHAMP, *J. Atmos. Sol.-Terr. Phys.*, *71*, 967–974, doi:10.1016/j.jastp.20.

Cheng, C., Y. Kuo, R. Anthes, and L. Wu (2006), Satellite constellation monitors global and space weather, *Eos Trans.*, *87*, 166.

de la Beaujardière, O., and C/NOFS Science Definition Team (2004), C/NOFS: A mission to forecast scintillations, *J. Atmos. Sol.-Terr. Phys.*, *66*, 1573–1591.

Forbes, J. M., X. Zhang, S. Palo, J. Russell, C. J. Mertens, and M. G. Mlynczak (2008), Tidal variability in the ionospheric dynamo region, *J. Geophys. Res.*, *113*, A02310, doi:10.1029/2007JA012737.

Hargreaves, J. K. (1994), *The Solar-Terrestrial Environment, Cambridge Atmospheric and Space Science Series,* vol. 5, 1st ed., Cambridge University Press, New York, NY (USA).

Heelis, R. A. (2004), Electrodynamics in the low and middle latitude ionosphere: A tutorial, *J. Atmos. Sol.-Terr. Phys.*, *66*, 825–838.

Heelis, R. A., and W. Hanson (1998), Measurements of thermal ion drift velocity and temperature using planar sensors, in *Measurement Techniques in Space Plasmas: Particles, Geophys. Monogr. Ser.,* vol. 102, edited by F. Pfaff, E. Borovsky, and T. Young, pp. 61–71, AGU, Washington, D. C., doi:10.1029/GM102p0061.

Heelis, R. A., and W. B. Hanson (1980), Interhemispheric transport induced by neutral zonal winds in the F region, *J. Geophys. Res.*, *85*(A6), 3045–3047.

Immel, T. J., E. Sagawa, S. L. England, S. B. Henderson, M. E. Hagan, S. B. Mende, H. U. Frey, C. M. Swenson, and L. J. Paxton (2006), Control of equatorial ionospheric morphology by atmospheric tides, *Geophys. Res. Lett.*, *33*, L15108, doi:10.1029/2006GL026161.

Kutiev, I., R. A. Heelis, and S. Sanatani (1980), The behavior of the O^+-H^+ transition level at solar maximum, *J. Geophys. Res.*, *85*(A5), 2366–2372.

Lin, C. H., C. C. Hsiao, J. Y. Liu, and C. H. Liu (2007), Longitudinal structure of the equatorial ionosphere: Time evolution of the four-peaked EIA structure, *J. Geophys. Res.*, *112*, A12305, doi:10.1029/2007JA012455.

Maus, S., et al. (2005), The 10^{th} Generation International Geomagnetic Reference Field, *Phys. Earth Planet. Inter.*, *151*, 320–322, doi:10.1016/j.pepi.2005.03.006.

Moffett, R. J., and W. B. Hanson (1973), Calculated distributions of hydrogen and helium ions in the low-latitude ionosphere, *J. Atmos. Terr. Phys.*, *35*(2), 207–222, doi:10.1016/0021-9169(73)90088-3.

Oberheide, J., and J. M. Forbes (2008), Tidal propagation of deep tropical cloud signatures into the thermosphere from TIMED observations, *Geophys. Res. Lett.*, *35*, L04816, doi:10.1029/2007GL032397.

Oyama, K., S. Watanabe, Y. Su, T. Takahashi, and K. Hirao (1996), Season, local time, and longitude variations of electron temperature at the height of ∼600 km in the low latitude region, *Adv. Space Res.*, *18*(6), 269–278, doi:10.1016/0273-1177(95)00936-1.

Pedatella, N. M., M. E. Hagan, and A. Maute (2012), The comparative importance of DE3, SE2, and SPW4 on the generation of wavenumber-4 longitude structures in the low-latitude ionosphere during September equinox, *Geophys. Res. Lett.*, *39*, L19108, doi:10.1029/2012GL053643.

Sagawa, E., T. J. Immel, H. U. Frey, and S. B. Mende (2005), Longitudinal structure of the equatorial anomaly in the nighttime ionosphere observed by IMAGE/FUV, *J. Geophys. Res.*, *110*, A11302, doi:10.1029/2004JA010848.

Stoneback, R. A., R. A. Heelis, A. G. Burrell, W. R. Coley, B. G. Fejer, and E. E. Pacheco Josán (2011), Observations of quiet time vertical ion drift in the equatorial ionosphere during the solar minimum period of 2009, *J. Geophys. Res.*, *116*, A12327, doi:10.1029/2011JA016712.

Su, Y., G. Bailey, and K. Oyama (1998), Annual and seasonal variations in the low-latitude topside ionosphere, *Ann. Geophys.*, *16*(8), 974–985.

Tulasi Ram, S., S.-Y. Su, and C. H. Liu (2009), FORMOSAT-3/COSMIC observations of seasonal and longitudinal variations of equatorial ionization anomaly and its interhemispheric asymmetry during the solar minimum period, *J. Geophys. Res.*, *114*, A06311, doi:10.1029/2008JA013880.

Venkatraman, S., and R. A. Heelis (1999), Effects of solar activity variations on adiabatic heating and cooling effects in the nighttime equatorial topside ionosphere, *J. Geophys. Res.*, *104*(A8), 17,117–17,126.

Venkatraman, S., and R. A. Heelis (2000), Interhemispheric plasma flows in the equatorial topside ionosphere, *J. Geophys. Res.*, *105*(A8), 18,457–18,464.

Wan, W., Z. Ren, F. Ding, J. Xiong, L. Liu, B. Ning, B. Zhao, G. Li, and M.-L. Zhang (2012), A simulation study for the couplings between DE3 tide and longitudinal WN4 structure in the thermosphere and ionosphere, *J. Atmos. Sol.-Terr. Phys.*, *90-91*, 52–60, doi:10.1016/j.jastp.2012.04.011.

West, K. H., and R. A. Heelis (1996), Longitude variations in ion composition in the morning and evening topside equatorial ionosphere near solar minimum, *J. Geophys. Res.*, *101*(A4), 7951–7960.

West, K. H., R. A. Heelis, and F. J. Rich (1997), Solar activity variations in the composition of the low-latitude topside ionosphere, *J. Geophys. Res.*, *102*(A1), 295–305.

Yue, X., W. Schreiner, J. Lei, S. Sokolovskiy, C. Rocken, D. Hunt, and Y. Kuo (2010), Error analysis of Abel retrieved electron density profiles from radio occultation measurements, *Ann. Geophys.*, *28*, 217–222.